Preprints of the 21st IFAC World Congress (Virtual)
Berlin, Germany, July 12-17, 2020

Comparative analysis for noise propagation in a coarse-grained model linking metabolism to cellular growth

A. Borri * **P. Palumbo** ** **A. Singh** ***

* *Istituto di Analisi dei Sistemi ed Informatica "A. Ruberti", Consiglio Nazionale delle Ricerche (IASI-CNR), BioMatLab - UCSC - Largo A. Gemelli 8, 00168 Roma, Italy. (e-mail: alessandro.borri@biomatematica.it)*
** *Department of Biotechnologies and Biosciences, University of Milano-Bicocca, Piazza della Scienza 2, 20126 Milan, Italy, Italy (e-mail: pasquale.palumbo@unimib.it)*
*** *Department of Electrical and Computer Engineering, Biomedical Engineering, Mathematical Sciences, Center for Bioinformatics and Computational Biology, University of Delaware, Newark, DE USA 19716 (e-mail: absingh@udel.edu)*

Abstract:
Fluctuations in growth rate have been shown to be important drivers of phenotypic heterogeneity. So far they have been usually related to gene expression or enzymatic reactions, since the metabolism was supposed to average the mixture of many and different noisy reactions involved in it. On the other hand, single-cell experiments have recently highlighted how noise may well propagate also from metabolic reactions, and influence cellular growth rate. In this work, a coarse-grained model of the relationships linking cellular resources to growth rate and metabolism is investigated with respect to noise propagation. An incoherent feedforward control is exerted by growth rate on metabolic enzymes, since growth is supposed to positively control both metabolic enzymes production and degradation. Different noise sources have been addressed, affecting metabolic production, cellular resource clearance and production. Noise sources have been addressed one at a time, and noise propagation has been investigated by means of a Stochastic Hybrid System model, whose shape is modulated according to the different noise sources. Results provide interesting biological insights about the causal relationship concerning noise propagation from growth to metabolism and vice versa.

Keywords: Metabolic pathways, Systems Biology, Stochastic Approach

1. INTRODUCTION

This work investigates how noise propagates in a coarse-grained model linking together metabolic enzymes, cellular resources and growth rate. Metabolism has been rarely involved in such analysis because of the many concurrent molecular patterns acting at the metabolic level, providing an average smoothing of the noise effects. On the other hand, recent single-cell investigations have gathered interest in metabolic noise, showing how fluctuations in gene expression and enzyme accumulation are tightly related to metabolic fluxes and growth rate (see, e.g. Kiviet et al. (2014); Nordholt et al. (2018); Wehrens et al. (2018); Thomas et al. (2018); Kleijn et al. (2018); Tonn et al. (2019); Weiße et al. (2015)).

The model under investigation considers a growing cell whose growth rate g is controlled by the accumulation of a set of cellular resources, represented by X in the scheme of Fig. 1. The growth rate in turn controls both the production and the clearance rate of a class of metabolic enzymes, represented by Y in Fig. 1. Indeed, the decay of molecular players is, generally, governed by dilution, strictly related to growth rate and, moreover, in the work of Klumpp et al. (2009) it is shown how growth rate positively regulates also the transcription rate.

Finally, Y closes the loop by properly regulating X production rate. In fact, such a scheme may be treated as an incoherent feedforward loop, since X controls (indirectly, by means of the growth rate g) both accumulation and degradation of Y, see Alon (2009); Soltani et al. (2016).

Three noise sources are here considered. One involves the enzyme Y production rate and the other two involve the clearance and production rate of the cellular resource X. A simplified scenario has been proposed in Borri et al. (2018), where a unique noise source (the one affecting Y) was considered to act on such a network.

Noise propagation is investigated by accounting for one noise source at a time. We build a class of Stochastic Hybrid System that entails the three frameworks in a unique fashion although, in some cases, noise is supposed to exert its action discretely, and in some other continuously. Since

we are interested in noise correlations between metabolism and cellular growth, we aim at investigating the cross-correlation functions, thus focusing our attention to first- and second-order moments. Although this fact unburden the computational load, a linear approximation is still required, otherwise moment equations are not closed and stationary values cannot be computed (see Hespanha & Singh (2005); Singh & Hespanha (2011); Sontag & Singh (2015)). The goodness of the analytical results, achieved according to the aforementioned approximation is validated by means of Monte Carlo random paths simulations, carried out by properly implementing the τ-leap version of the Gillespie algorithm (in case of discrete noise) (see Gillespie (1977, 2001)) or the Euler-Maruyama integration method for stochastic differential equations, in case of continuous noise, Higham (2001).

Results highlight how different noise sources provide different and opposite causal relationships. For instance, if noise affects the production of metabolic enzymes, it is reasonable to expect that it propagates from metabolism to cellular growth, since growth is positively controlled by cellular resource accumulation, whose production rate is positively controlled by the metabolic enzymes. Indeed, such results had been highlighted in Borri et al. (2018) and experimentally confirmed in Wehrens et al. (2018). Less intuitive is how metabolism correlates to growth if the noise source is constrained to cellular resource production or degradation. In this case, the incoherent feedforward control exerted by growth on both production and clearance rate of metabolic enzymes prevents to make a straightforward prediction, and computations are invoked to unravel the mechanism. Provided results show a negative correlation for both these other two cases.

2. MODEL SETTING

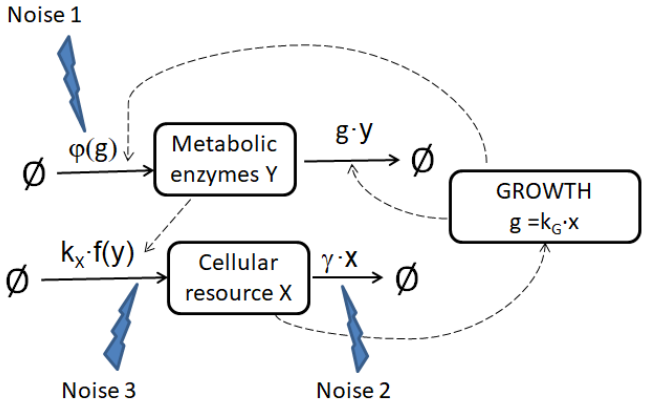

Fig. 1. Scheme of the metabolic coarse-grained model. Model 1 refers to only Noise 1 affecting the metabolic enzymes production rate; Model 2 refers to only Noise 2 affecting the clearance rate of the cellular resource; Model 3 refers to only Noise 3 affecting the cellular resource production rate.

As reported in the Introduction, three distinct models are considered, each related to a specific noise source. For the three models, X and Y will be described by means of their copy numbers $\mathbf{x}$ and $\mathbf{y}$. Model 1 refers to the noise related to the production of the metabolic enzyme Y (*Noise 1*), which is supposed to occur in discrete bursts of η copy numbers. The size η of the burst is a discrete random variable taking values in $\{1, 2, \ldots\}$ according to a chosen probability distribution $\mathbb{P}(\eta = j)$, $j = 0, 1, \ldots$, like in Soltani et al. (2015); Golding et al. (2005). The average size of η will be shortly denoted by $\overline{\eta}$. The growth rate exerts a feedback on the metabolic enzyme production, since we assume that the propensity a_j of an event of j bursts production depends on the growth rate according to a nonlinear saturating function $\varphi(g)$, chosen to be monotonically increasing (e.g. a saturating exponential or a Michaelis-Menten, according to the experimental results in Klumpp et al. (2009)). Moreover, the relationship between the cellular resource X and the growth rate g is supposed linear:

$$g(\mathbf{x}) = k_G \mathbf{x}. \tag{1}$$

Therefore, for any $j = 1, 2, \ldots$:

$$Y \mapsto Y + j \qquad a_j(\mathbf{x}) = \varphi_g(\mathbf{x}) \mathbb{P}(\eta = j), \tag{2}$$

with

$$\varphi_g(\mathbf{x}) = \varphi\big(g(\mathbf{x})\big) = \varphi\big(k_G \mathbf{x}\big). \tag{3}$$

With a little abuse of notation ($\mathbf{x}$ and $\mathbf{y}$ are discrete copy numbers) within any two consecutive bursts, the X and Y dynamics evolve continuously according to the following Ordinary Differential Equation (ODE) model:

$$\begin{cases} \dot{\mathbf{x}} &= k_X f(\mathbf{y}) - \overline{\gamma} \mathbf{x} \\ \dot{\mathbf{y}} &= -k_G \mathbf{x} \mathbf{y} \end{cases} \tag{4}$$

Such a Stochastic Hybrid System model has been investigated in Borri et al. (2018).

Model 2 addresses the noise source affecting the clearance of X, by modeling such a clearance rate $\boldsymbol{\gamma}$ as an Ornstein-Uhlenbeck (UO) process, i.e. $\boldsymbol{\gamma}$ obeys to the following linear Stochastic Differential Equation (SDE):

$$d\boldsymbol{\gamma} = \theta(\overline{\gamma} - \boldsymbol{\gamma}) dt + \sigma dW_t \tag{5}$$

with $\overline{\gamma}$ readily shown to provide the steady-state average value. W_t is a standard Wiener process (zero-mean and unitary variance). By assuming the stochasticity of only *Noise 2*, the whole system is supposed to evolve according to the following SDE:

$$\begin{cases} d\mathbf{x} &= k_X f(\mathbf{y}) dt - \boldsymbol{\gamma} \mathbf{x} dt \\ d\boldsymbol{\gamma} &= \theta(\overline{\gamma} - \boldsymbol{\gamma}) dt + \sigma dW_t \\ d\mathbf{y} &= -k_G \mathbf{x} \mathbf{y} dt + \overline{\eta} \varphi_g(\mathbf{x}) dt \end{cases} \tag{6}$$

where $\overline{\eta}$ is the average value of the random variable describing the size of the bursts for the noisy enzyme production in Model 1.

Finally, Model 3 accounts for only *Noise 3* and considers X production rate as the following discrete update

$$X \mapsto X + 1, \qquad a(\mathbf{y}) = k_X f(\mathbf{y}) \tag{7}$$

with $a(\mathbf{y})$ the propensity of a unitary update ruled by the metabolic enzyme accumulation by means of the saturating function $f(\mathbf{y})$. Between any two production events, similarly to Model 1, the system evolves continuously according to the following ODE system

$$\begin{cases} \dot{\mathbf{x}} &= -\overline{\gamma} \mathbf{x} \\ \dot{\mathbf{y}} &= -k_G \mathbf{x} \mathbf{y} + \overline{\eta} \varphi_g(\mathbf{x}) \end{cases} \tag{8}$$

The three models could be formally written according to a unifying Stochastic Hybrid System formalism, where the continuous part dynamics is rendered by the following SDE

$$d\mathbf{z} = h(\mathbf{z})dt + \beta(\mathbf{z})dW \tag{9}$$

with $\mathbf{z} = [\mathbf{x}\ \ \mathbf{y}]^T$ for Models 1 and 3, whilst $\mathbf{z} = [\mathbf{x}\ \ \boldsymbol{\gamma}\ \ \mathbf{y}]^T$ for Model 2. Clearly, functions $h(\cdot)$ and $\beta(\cdot)$ have different shapes according to the different models

– Model 1:
$$\begin{aligned} h(\mathbf{z}) &= (k_X f(\mathbf{z}_2) - \overline{\gamma}\mathbf{z}_1 \quad - k_G \mathbf{z}_1\mathbf{z}_2)^T \\ \beta(\mathbf{z}) &= (0 \quad 0)^T \end{aligned} \tag{10}$$

– Model 2:
$$\begin{aligned} h(\mathbf{z}) = \big(k_X f(\mathbf{z}_3) - \mathbf{z}_1\mathbf{z}_2 \quad \theta(\overline{\gamma} - \mathbf{z}_2) \\ -k_G\mathbf{z}_1\mathbf{z}_3 + \overline{\eta}\varphi_g(\mathbf{z}_1)\big)^T \\ \beta(\mathbf{z}) = (0 \quad \sigma \quad 0)^T \end{aligned} \tag{11}$$

– Model 3:
$$\begin{aligned} h(\mathbf{z}) &= (-\overline{\gamma}\mathbf{z}_1 \quad - k_G\mathbf{z}_1\mathbf{z}_2 + \overline{\eta}\varphi_g(\mathbf{z}_1))^T \\ \beta(\mathbf{z}) &= (0 \quad 0)^T \end{aligned} \tag{12}$$

Within the SHS formalism, the SDE is endowed with the following set of stochastic discrete reset maps:

$$Z \mapsto Z + \Delta_j, \quad \text{propensity} \quad a_j(\mathbf{z}), \quad j \in \mathcal{J} \tag{13}$$

In case of Model 1, we have

$$\Delta_j = [0 \ \ j]^T, \quad a_j(\mathbf{z}) = \varphi_g(\mathbf{z}_1)\mathbb{P}(\eta = j), \quad j = 1, 2, \dots \tag{14}$$

in case of Model 2 we have no discrete resets and $\mathcal{J} = \emptyset$ whilst, in case of Model 3, we have

$$\Delta_1 = [1 \ \ 0]^T, \quad a_1(\mathbf{z}) = k_X f(\mathbf{z}_2). \tag{15}$$

3. FIRST-ORDER MOMENTS

According to the SHS of the type (9), (13), finite-order moments dynamics is written by means of the following general formula provided by Hespanha & Singh (2005) for a general nonlinear function $\psi(\cdot)$:

$$\begin{aligned} \frac{d}{dt}\langle\psi(\mathbf{z})\rangle = \Big\langle\frac{d\psi}{d\mathbf{z}}h(\mathbf{z})\Big\rangle + \sum_{j=1}^{\infty}\big\langle\big(\psi(\mathbf{z}+\Delta_j) - \psi(\mathbf{z})\big)a_j(\mathbf{z})\big\rangle \\ + \frac{1}{2}\text{trace}\left(\frac{\mathrm{d}^2\psi}{d\mathbf{z}^2}\beta(\mathbf{z})\beta^T(\mathbf{z})\right) \end{aligned} \tag{16}$$

Because of nonlinearities in $h(\cdot)$ and $a_j(\cdot)$, moment equations are not available in closed form, therefore we need to resort to moment closure techniques, Singh & Hespanha (2011), or to linear noise approximations for SHS, Modi et al. (2018). Within this framework, in order to find analytical results, we consider the linearization around the stationary average values $\overline{x}$, $\overline{\gamma}$, $\overline{y}$ of the nonlinear functions involved in the models, i.e.:

$$\varphi_g(\mathbf{x}) \simeq \varphi_g(\overline{x}) + \varphi_g'(\overline{x})(\mathbf{x} - \overline{x}) \tag{17}$$

$$\mathbf{xy} \simeq \overline{x}\,\overline{y} + \overline{y}(\mathbf{x} - \overline{x}) + \overline{x}(\mathbf{y} - \overline{y}) \tag{18}$$

$$\boldsymbol{\gamma}\mathbf{x} \simeq \overline{\gamma}\,\overline{x} + \overline{\gamma}(\mathbf{x} - \overline{x}) + \overline{x}(\boldsymbol{\gamma} - \overline{\gamma}) \tag{19}$$

$$f(\mathbf{y}) \simeq f(\overline{y}) + f'(\overline{y})(\mathbf{y} - \overline{y}) \tag{20}$$

Dealing with the first-order moments, formula (16) is written with $\psi(\mathbf{z}) = \mathbf{z}$. By properly substituting (17)-(20) into (16), we have, after computations:

$$\frac{d}{dt}\langle\mathbf{z}\rangle = A_i(\overline{x}, \overline{\gamma}, \overline{y})\langle\mathbf{z}\rangle + b_i(\overline{x}, \overline{\gamma}, \overline{y}), \tag{21}$$

with pairs (A_i, b_i), $i = 1, 2, 3$ associated to Model i:

$$A_1(\overline{x}, \overline{\gamma}, \overline{y}) = A_3(\overline{x}, \overline{\gamma}, \overline{y}) = \begin{bmatrix} -\overline{\gamma} & k_X f'(\overline{y}) \\ \overline{\eta}\varphi_g'(\overline{x}) - k_G\overline{y} & -k_G\overline{x} \end{bmatrix} \tag{22}$$

$$b_1(\overline{x}, \overline{\gamma}, \overline{y}) = b_3(\overline{x}, \overline{\gamma}, \overline{y}) \begin{bmatrix} k_X\big(f(\overline{y}) - f'(\overline{y})\overline{y}\big) \\ \overline{\eta}\varphi_g(\overline{x}) + \big(k_G\overline{y} - \overline{\eta}\varphi_g'(\overline{x})\big)\overline{x} \end{bmatrix}, \tag{23}$$

$$A_2(\overline{x}, \overline{\gamma}, \overline{y}) = \begin{bmatrix} -\overline{\gamma} & -\overline{x} & k_X f'(\overline{y}) \\ 0 & -\theta & 0 \\ \overline{\eta}\varphi_g'(\overline{x}) - k_G\overline{y} & 0 & -k_G\overline{x} \end{bmatrix} \tag{24}$$

$$b_2(\overline{x}, \overline{\gamma}, \overline{y}) = \begin{bmatrix} k_X\big(f(\overline{y}) - f'(\overline{y})\overline{y}\big) + \overline{\gamma}\,\overline{x} \\ \theta\overline{\gamma} \\ \overline{\eta}\varphi_g(\overline{x}) + \big(k_G\overline{y} - \overline{\eta}\varphi_g'(\overline{x})\big)\overline{x} \end{bmatrix}. \tag{25}$$

With regards to Model 1, we have shown in Borri et al. (2018) that:

– if $\varphi_g(\overline{x})/\overline{x}$ is a monotonically decreasing function in $\overline{x} \geq 0$, with
$$\lim_{\overline{x}\mapsto 0^+}\frac{\varphi_g(\overline{x})}{\overline{x}} = M > 0, \tag{26}$$
then there exists a unique nontrivial, positive solution for the pair $(\overline{x}, \overline{y})$;
– moreover, if $f(\overline{y})/\overline{y}$ is a monotonically decreasing function for $\overline{y} \geq 0$, then, the ODE system describing the first-order moment equation of the linearized system is Hurwitz.

An analogous result for the stationary values $\overline{x}$ and $\overline{y}$ and for the stability of the linearized system comes out when dealing with Model 2 and Model 3. Indeed, Model 3 actually shares the same first-order dynamics with Model 1. In regards to Model 2, it readily comes that $\boldsymbol{\gamma}$ dynamics is achieved independently of $\mathbf{x}$ and $\mathbf{y}$ with $\langle\boldsymbol{\gamma}\rangle \mapsto \overline{\gamma}$, so that, at steady-state, the $\overline{x}$ and $\overline{y}$ obey to the same algebraic constraint for the 3 models, i.e.

$$A_1(\overline{x}, \overline{\gamma}, \overline{y})\begin{bmatrix}\overline{x}\\ \overline{y}\end{bmatrix} + b_1(\overline{x}, \overline{\gamma}, \overline{y}) = 0. \tag{27}$$

In summary, the three models share the same first-order analysis. The next Section highlights the differences arising when dealing second-order moments.

4. SECOND-ORDER MOMENTS AND CROSS-/AUTOCORRELATIONS

Here we compute the second-order moments, in order to build the cross-correlation functions, required to infer information on whether noise fluctuations propagate from the metabolic enzyme Y on cellular growth, or vice versa. According to formula (16), second-order moments are written by setting function $\psi(\mathbf{z}) = \mathbf{z}_i\mathbf{z}_j$, $i, j = 1, 2, 3$.

Concerning Model 1, computations have been carried out in Borri et al. (2018), providing the steady-state solutions $\overline{\langle\mathbf{x}^2\rangle}$, $\overline{\langle\mathbf{y}^2\rangle}$, $\overline{\langle\mathbf{xy}\rangle}$ as the solutions of the following linear system:

$$\begin{aligned} \Gamma^1_{x^2}\Big(\overline{\langle\mathbf{x}^2\rangle}, \overline{\langle\mathbf{xy}\rangle}\Big) = 0 \\ \Gamma^1_{y^2}\Big(\overline{\langle\mathbf{y}^2\rangle}, \overline{\langle\mathbf{xy}\rangle}\Big) = 0 \\ \Gamma^1_{xy}\Big(\overline{\langle\mathbf{x}^2\rangle}, \overline{\langle\mathbf{y}^2\rangle}, \overline{\langle\mathbf{xy}\rangle}\Big) = 0 \end{aligned} \tag{28}$$

where

$$\begin{aligned} \Gamma^1_{x^2}\Big(\overline{\langle\mathbf{x}^2\rangle}, \overline{\langle\mathbf{xy}\rangle}\Big) = k_X\overline{x}\,\overline{y}\left(\frac{f(\overline{y})}{\overline{y}} - f'(\overline{y})\right) - \overline{\gamma}\overline{\langle\mathbf{x}^2\rangle} \\ + k_X f'(\overline{y})\overline{\langle\mathbf{xy}\rangle} \end{aligned} \tag{29}$$

$$\Gamma^1_{y^2}\Big(\overline{\langle \mathbf{y}^2\rangle}, \overline{\langle \mathbf{xy}\rangle}\Big) = \frac{\langle \eta^2\rangle}{2}\varphi_g(\overline{x}) + \overline{x}\,\overline{y}\,\overline{\eta}\left(2\frac{\varphi_g(\overline{x})}{\overline{x}} - \varphi'_g(\overline{x})\right) - k_G\overline{x}\overline{\langle \mathbf{y}^2\rangle} - \overline{\eta}\left(\frac{\varphi_g(\overline{x})}{\overline{x}} - \varphi'_g(\overline{x})\right)\overline{\langle \mathbf{xy}\rangle} \tag{30}$$

$$\Gamma^1_{xy}\Big(\overline{\langle \mathbf{y}^2\rangle}, \overline{\langle \mathbf{xy}\rangle}\Big) = k_X f'(\overline{y})\overline{\langle \mathbf{y}^2\rangle} - (\overline{\gamma} + k_G\overline{x})\overline{\langle \mathbf{xy}\rangle} - \overline{\eta}\left(\frac{\varphi_g(\overline{x})}{\overline{x}} - \varphi'_g(\overline{x})\right)\overline{\langle \mathbf{x}^2\rangle} + k_X\overline{y}^2\left(\frac{f(\overline{y})}{\overline{y}} - f'(\overline{y})\right) + \overline{\eta}\,\overline{x}^2\left(2\frac{\varphi_g(\overline{x})}{\overline{x}} - \varphi'_g(\overline{x})\right). \tag{31}$$

In relation to Model 2, we have $\overline{\langle \mathbf{x}^2\rangle}$, $\overline{\langle \mathbf{y}^2\rangle}$, $\overline{\langle \mathbf{xy}\rangle}$, as the solutions of the following linear system:

$$\begin{aligned}\Gamma^2_{x^2}\Big(\overline{\langle \mathbf{x}^2\rangle}, \overline{\langle \mathbf{xy}\rangle}, \overline{\langle \mathbf{x}\boldsymbol{\gamma}\rangle}\Big) &= 0\\ \Gamma^2_{y^2}\Big(\overline{\langle \mathbf{y}^2\rangle}, \overline{\langle \mathbf{xy}\rangle}\Big) &= 0\\ \Gamma^2_{xy}\Big(\overline{\langle \mathbf{x}^2\rangle}, \overline{\langle \mathbf{y}^2\rangle}, \overline{\langle \mathbf{xy}\rangle}, \overline{\langle \mathbf{y}\boldsymbol{\gamma}\rangle}\Big) &= 0\end{aligned} \tag{32}$$

where

$$\Gamma^2_{x^2}\Big(\overline{\langle \mathbf{x}^2\rangle}, \overline{\langle \mathbf{xy}\rangle}, \overline{\langle \mathbf{x}\boldsymbol{\gamma}\rangle}\Big) = \Gamma^1_{x^2}\Big(\overline{\langle \mathbf{x}^2\rangle}, \overline{\langle \mathbf{xy}\rangle}\Big) + \overline{x}^2\overline{\gamma} - \overline{x}\overline{\langle \mathbf{x}\boldsymbol{\gamma}\rangle} \tag{33}$$

$$\Gamma^2_{y^2}\Big(\overline{\langle \mathbf{y}^2\rangle}, \overline{\langle \mathbf{xy}\rangle}\Big) = \Gamma^1_{y^2}\Big(\overline{\langle \mathbf{y}^2\rangle}, \overline{\langle \mathbf{xy}\rangle}\Big) - \frac{\langle \eta^2\rangle}{2}\varphi_g(\overline{x}) \tag{34}$$

$$\Gamma^2_{xy}\Big(\overline{\langle \mathbf{y}^2\rangle}, \overline{\langle \mathbf{xy}\rangle}, \overline{\langle \mathbf{y}\boldsymbol{\gamma}\rangle}\Big) = \Gamma^1_{xy}\Big(\overline{\langle \mathbf{y}^2\rangle}, \overline{\langle \mathbf{xy}\rangle}\Big) + \overline{x}\big(\overline{\gamma y} - \overline{\langle \boldsymbol{\gamma}\mathbf{y}\rangle}\big) \tag{35}$$

and second-order moments $\overline{\langle \mathbf{x}\boldsymbol{\gamma}\rangle}$ and $\overline{\langle \mathbf{y}\boldsymbol{\gamma}\rangle}$ come from the solutions of the following linear system

$$\begin{aligned}\Gamma^2_{x\gamma}\Big(\overline{\langle \mathbf{x}\boldsymbol{\gamma}\rangle}, \overline{\langle \mathbf{y}\boldsymbol{\gamma}\rangle}\Big) &= 0\\ \Gamma^2_{y\gamma}\Big(\overline{\langle \mathbf{x}\boldsymbol{\gamma}\rangle}, \overline{\langle \mathbf{y}\boldsymbol{\gamma}\rangle}\Big) &= 0\end{aligned} \tag{36}$$

where

$$\Gamma^2_{x\gamma}\Big(\overline{\langle \mathbf{x}\boldsymbol{\gamma}\rangle}, \overline{\langle \mathbf{y}\boldsymbol{\gamma}\rangle}\Big) = \overline{x}\overline{\langle \boldsymbol{\gamma}^2\rangle} + \overline{\gamma}\overline{\langle \mathbf{x}\boldsymbol{\gamma}\rangle} - 2\overline{x\gamma}^2 + k_X f'(\overline{y})\overline{\gamma y} - \theta\overline{x\gamma} + \theta\overline{\langle \mathbf{x}\boldsymbol{\gamma}\rangle} - k_X f'(\overline{y})\overline{\langle \mathbf{y}\boldsymbol{\gamma}\rangle} \tag{37}$$

$$\Gamma^2_{y\gamma}\Big(\overline{\langle \mathbf{x}\boldsymbol{\gamma}\rangle}, \overline{\langle \mathbf{y}\boldsymbol{\gamma}\rangle}\Big) = k_G\overline{y}\overline{\langle \mathbf{x}\boldsymbol{\gamma}\rangle} + k_G\overline{x}\overline{\langle \mathbf{y}\boldsymbol{\gamma}\rangle} - k_G\overline{xy\gamma} - \overline{\eta}\varphi_g(\overline{x})\overline{\gamma} - \overline{\eta}\varphi'_g(\overline{x})\overline{\langle \mathbf{x}\boldsymbol{\gamma}\rangle} + \overline{\eta}\varphi'_g(\overline{x})\overline{\gamma x} - \theta\big(\overline{\gamma\gamma} - \overline{\langle \boldsymbol{\gamma}\boldsymbol{\gamma}\rangle}\big) \tag{38}$$

and

$$\overline{\langle \boldsymbol{\gamma}^2\rangle} = \overline{\gamma}^2 + \frac{\sigma^2}{2\theta}. \tag{39}$$

With regards to Model 3, we have $\overline{\langle \mathbf{x}^2\rangle}$, $\overline{\langle \mathbf{y}^2\rangle}$, $\overline{\langle \mathbf{xy}\rangle}$, as the solutions of the following linear system:

$$\begin{aligned}\Gamma^3_{x^2}\Big(\overline{\langle \mathbf{x}^2\rangle}, \overline{\langle \mathbf{xy}\rangle}, \overline{\langle \mathbf{x}\boldsymbol{\gamma}\rangle}\Big) &= 0\\ \Gamma^3_{y^2}\Big(\overline{\langle \mathbf{y}^2\rangle}, \overline{\langle \mathbf{xy}\rangle}\Big) &= 0\\ \Gamma^3_{xy}\Big(\overline{\langle \mathbf{x}^2\rangle}, \overline{\langle \mathbf{y}^2\rangle}, \overline{\langle \mathbf{xy}\rangle}, \overline{\langle \mathbf{y}\boldsymbol{\gamma}\rangle}\Big) &= 0\end{aligned} \tag{40}$$

where

$$\Gamma^3_{x^2}\Big(\overline{\langle \mathbf{x}^2\rangle}, \overline{\langle \mathbf{xy}\rangle}, \overline{\langle \mathbf{x}\boldsymbol{\gamma}\rangle}\Big) = \Gamma^1_{x^2}\Big(\overline{\langle \mathbf{x}^2\rangle}, \overline{\langle \mathbf{xy}\rangle}\Big) + \frac{k_X}{2}f(\overline{y}) \tag{41}$$

$$\Gamma^3_{y^2}\Big(\overline{\langle \mathbf{y}^2\rangle}, \overline{\langle \mathbf{xy}\rangle}\Big) = \Gamma^1_{y^2}\Big(\overline{\langle \mathbf{y}^2\rangle}, \overline{\langle \mathbf{xy}\rangle}\Big) - \frac{\langle \eta^2\rangle}{2}\varphi_g(\overline{x}) \tag{42}$$

$$\Gamma^3_{xy}\Big(\overline{\langle \mathbf{y}^2\rangle}, \overline{\langle \mathbf{xy}\rangle}\Big) = \Gamma^1_{xy}\Big(\overline{\langle \mathbf{y}^2\rangle}, \overline{\langle \mathbf{xy}\rangle}\Big). \tag{43}$$

The cross-correlation coefficient associated to the pair $(\mathbf{y}, g)$ is defined as follows

$$\rho_{yg}(\tau) = \frac{\overline{\langle \mathbf{y}(t)g(t+\tau)\rangle} - \overline{y}g(\overline{x})}{\sigma_Y\sigma_g}, \tag{44}$$

where $\tau \in \mathbb{R}$ is the lag, describing a delay related to noise propagation, and σ_Y, σ_g are the stationary standard deviations associated to Y and g, respectively, with

$$\sigma_g^2 = \overline{\Big\langle \big(g(\mathbf{x}) - \overline{\langle g(x)\rangle}\big)^2\Big\rangle} = \overline{\Big\langle k_G^2\big(\mathbf{x} - \overline{x}\big)^2\Big\rangle} = k_G^2\sigma_X^2. \tag{45}$$

In summary, the cross-correlation function for the pair $(\mathbf{y}, g)$ is:

$$\rho_{yg}(\tau) = \frac{\overline{\langle \mathbf{y}(t)\mathbf{x}(t+\tau)\rangle} - \overline{x}\,\overline{y}}{\sigma_X\sigma_Y} = \rho_{yx}(\tau). \tag{46}$$

Computations for the case of $\tau \geq 0$ and $\tau < 0$ follow the same line of Singh & Bokes (2012); Borri et al. (2018). Therefore, for $\tau \geq 0$ we exploit the relationship

$$\langle \mathbf{y}(t)\mathbf{x}(t+\tau)\rangle = \langle \mathbf{y}(t)\,\langle \mathbf{x}(t+\tau)|\mathbf{z}(t)\rangle\rangle \tag{47}$$

where $\mathbf{z}$ is the vector defined in Section 2 entailing the pair $\mathbf{x}$, $\mathbf{y}$ for Models 1, 3 or the triple $\mathbf{x}$, $\boldsymbol{\gamma}$, $\mathbf{y}$ for Model 2. Then,

$$\langle \mathbf{x}(t+\tau)|\mathbf{z}(t)\rangle = C_{xi}e^{A_i\tau}\mathbf{z}(t) + C_{xi}A_i^{-1}\big(e^{A_i\tau} - I\big)b_i \tag{48}$$

with $C_{xi} = [1\ \ 0]$ for $i = 1, 3$ and $C_{xi} = [1\ \ 0\ \ 0]$ for $i = 2$, provided that A_i is invertible. If we substitute (48) into (47), it is

$$\langle \mathbf{y}(t)\mathbf{x}(t+\tau)\rangle = C_{xi}e^{A_i\tau}\,\langle \mathbf{y}(t)\mathbf{z}(t)\rangle + \langle \mathbf{y}(t)\rangle\, C_{xi}A_i^{-1}\big(e^{A_i\tau} - I\big)b_i \tag{49}$$

so that, at steady-state

$$\overline{\langle \mathbf{y}(t)\mathbf{x}(t+\tau)\rangle} = C_{xi}e^{A_i\tau}\overline{\langle \mathbf{yz}\rangle} + \overline{y}C_{xi}A^{-1}\big(e^{A_i\tau} - I\big)b_i \tag{50}$$

with

$$\overline{\langle \mathbf{yz}\rangle} = \Big[\overline{\langle \mathbf{xy}\rangle} \quad \overline{\langle \mathbf{y}^2\rangle}\Big]^T \tag{51}$$

for Model 1, 3, whilst

$$\overline{\langle \mathbf{yz}\rangle} = \Big[\overline{\langle \mathbf{xy}\rangle} \quad \overline{\langle \boldsymbol{\gamma}\mathbf{y}\rangle} \quad \overline{\langle \mathbf{y}^2\rangle}\Big]^T \tag{52}$$

for Model 2. On the other hand, for $\tau < 0$, we have:

$$\langle \mathbf{y}(t)\mathbf{x}(t+\tau)\rangle = \langle \mathbf{y}(t)\mathbf{x}(t-|\tau|)\rangle = \big\langle \mathbf{x}(t-|\tau|)\,\langle \mathbf{y}(t)|\mathbf{z}(t-|\tau|)\rangle\,\big\rangle \tag{53}$$

and so, at steady-state:

$$\overline{\langle \mathbf{y}(t)\mathbf{x}(t+\tau)\rangle} = \overline{\langle \mathbf{x}(t)\mathbf{y}(t+|\tau|)\rangle}. \tag{54}$$

Then, dealing with $\langle \mathbf{x}(t)\mathbf{y}(t+|\tau|)\rangle$, it is

$$\langle \mathbf{x}(t)\mathbf{y}(t+|\tau|)\rangle = \big\langle \mathbf{x}(t)\,\langle \mathbf{y}(t+|\tau|)|\mathbf{z}(t)\rangle\,\big\rangle. \tag{55}$$

so that, according to (21), we have:

$$\langle \mathbf{y}(t+|\tau|)|\mathbf{z}(t)\rangle = C_{yi}e^{A_i|\tau|}\mathbf{z}(t) + C_{yi}\int_t^{t+|\tau|} e^{A_i(t+|\tau|-s)}b_i\,ds \tag{56}$$

with $C_{yi} = [0\ \ 1]$ for $i = 1, 3$ and $C_{xi} = [0\ \ 0\ \ 1]$ for $i = 2$, that becomes

$$\langle \mathbf{y}(t+|\tau|)|\mathbf{z}(t)\rangle = C_{yi}e^{A_i|\tau|}\mathbf{z}(t) + C_{yi}A_i^{-1}\big(e^{A_i|\tau|} - I\big)b_i \tag{57}$$

provided that A_i is nonsingular. By substituting (57) into (55):

$$\langle \mathbf{x}(t)\mathbf{y}(t+|\tau|)\rangle = C_{yi}e^{A_i|\tau|}\,\langle \mathbf{x}(t)\mathbf{z}(t)\rangle + \langle \mathbf{x}(t)\rangle\, C_{yi}A_i^{-1}\big(e^{A_i|\tau|} - I\big)b_i \tag{58}$$

Table 1. Model parameters.

Parameter	Value	Parameter	Value
λ	0.2	k_X	1000
θ_F	300	$\bar{\gamma}$	1
θ_Y	500	k_G	$2 \cdot 10^{-4}$
k_Y	15	θ	1
σ	0.2		

and so, accounting for the steady-state solutions, when $t \mapsto +\infty$ we have

$$\overline{\langle \mathbf{x}(t)\mathbf{y}(t+|\tau|)\rangle} = C_{yi} e^{A_i|\tau|} \overline{\langle \mathbf{xz}\rangle} + \overline{x} C_{yi} A_i^{-1} \left(e^{A_i|\tau|} - I\right) b_i \tag{59}$$

with

$$\overline{\langle \mathbf{xz}\rangle} = \left[\overline{\langle \mathbf{x}^2\rangle} \quad \overline{\langle \mathbf{xy}\rangle}\right]^T \tag{60}$$

for Model 1, 3, and

$$\overline{\langle \mathbf{xz}\rangle} = \left[\overline{\langle \mathbf{x}^2\rangle} \quad \overline{\langle \mathbf{x\gamma}\rangle} \quad \overline{\langle \mathbf{xy}\rangle}\right]^T \tag{61}$$

for Model 2.

5. NUMERICAL SIMULATIONS

We here provide numerical simulations for the three models illustrated in the previous Sections. As in Borri et al. (2018), the nonlinear functions $f(\cdot)$ and $\varphi_g(\cdot)$ have been chosen as Michaelis-Menten functions

$$f(\mathbf{y}) = \frac{\mathbf{y}}{\mathbf{y} + \theta_F}, \qquad \varphi_g(\mathbf{x}) = k_Y \frac{\mathbf{x}}{\mathbf{x} + \theta_Y}, \tag{62}$$

satisfying $\varphi_g(\overline{\mathbf{x}})/\overline{\mathbf{x}}$ and $f(\overline{\mathbf{y}})/\overline{\mathbf{y}}$ to be monotonically decreasing functions.

With respect to the bursty noisy production of Y, as in Soltani et al. (2015); Borri et al. (2016, 2018), we assume the following geometric probability distribution:

$$\mathbb{P}(\eta = j) = (1-\lambda)^j \lambda, \qquad \lambda \in (0,1], \qquad j = 0, 1, \ldots \tag{63}$$

providing an average burst size $\overline{\eta} = (1-\lambda)/\lambda$.

Table 1 reports the set of model parameters, according to which the steady-state solutions provided by (27) are $\overline{x} = \theta_Y = 500$, $\overline{y} = \theta_F = 300$ (parameters set to provide steady-state values equal to the Michaelis-Menten constants), such that $\varphi_g(\overline{x}) = k_Y/2$ and $f(\overline{y}) = 1/2$.

A step selection of 0.1 seconds and an overall simulation time of 10,000 seconds has been chosen for both the τ-leaping algorithm of Gillespie (2001), employed for simulating Models 1 and 3, and for the Euler-Maruyama method chosen for integrating the SDE in Model 2, Higham (2001). In all cases, the ergodic properties of the underlying stochastic process have been exploited in order to infer the statistics of interest from the corresponding time averages.

Figs. 2–4 draw the cross-correlations according to the aforementioned scheme. It can be appreciated that the approximate analytical computations are validated by numerical simulations since there is a very good overlapping of the two curves (the numerical one, clearly obtained without any approximation, and the one achieved according to analytical computations carried out in Section 4). Differently from the results related to Model 1, providing a positive cross-correlation function with an apparent positive delay of the maximum (see Borri et al. (2018) where a discussion about Model 1 is given), the other

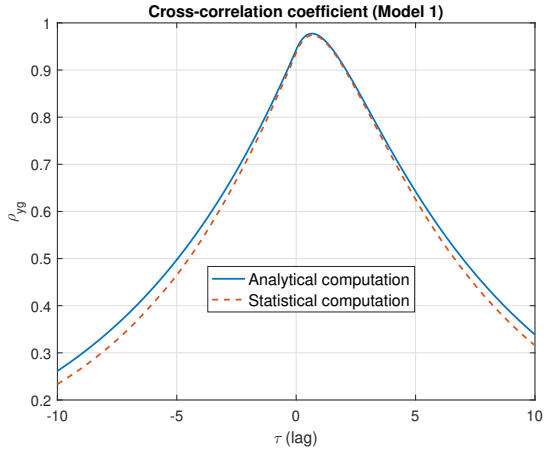

Fig. 2. Model 1: Cross-correlation function $\rho_{yg}(\tau)$ drawn according to the parameter values in Table 1. The approximate analytical computations (solid line) are validated by the statistical results obtained by means of the τ-leaping method (dashed line).

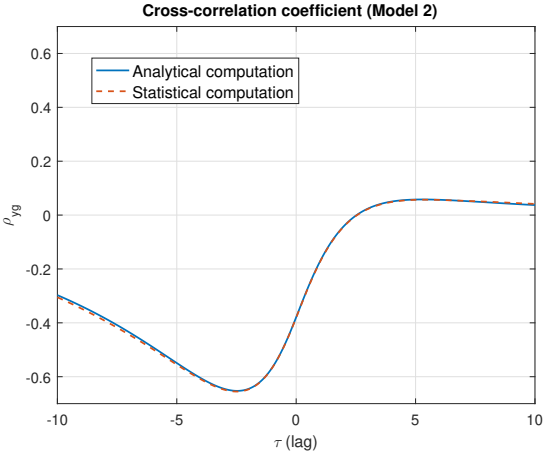

Fig. 3. Model 2: Cross-correlation function $\rho_{yg}(\tau)$ drawn according to the parameter values in Table 1. The approximate analytical computations (solid line) are validated by the statistical results obtained by means of the Euler-Maruyama method (dashed line).

two cross-correlation functions share a different behavior. Indeed, both show a trivial correlation for positive lags and a negative correlation for negative lags. The trivial correlation for positive lags suggests that, contrary to Model 1, in both Models 2 and 3, there seem to be no noise propagation from the metabolic enzymes to growth rate. On the other hand, noise seems to propagate with a non-trivial negative correlation from cellular growth to the metabolic enzyme. This fact could be explained by the incoherent feedforward control exerted by growth on both production and clearance rate of the metabolic enzymes. In summary, similarly to what comes out from the experimental results published in Kiviet et al. (2014), fluctuations may propagate from metabolism to growth and vice versa: growth noise may affect gene expression. Further investigation would require the building of an experimental setting aiming at confirming what the model predicts.

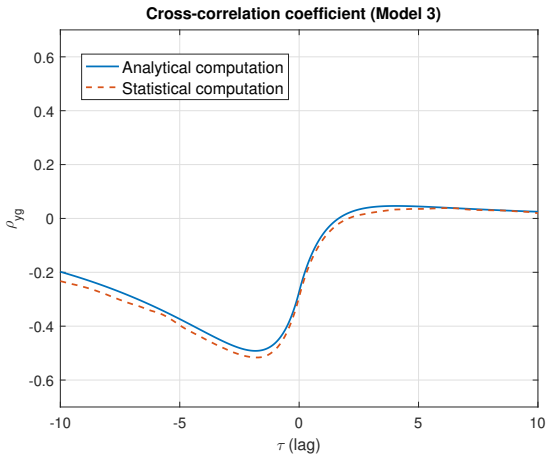

Fig. 4. Model 3: Cross-correlation function $\rho_{yg}(\tau)$ drawn according to the parameter values in Table 1. The approximate analytical computations (solid line) are validated by the statistical results obtained by means of the τ-leaping method (dashed line).

6. CONCLUSIONS

This work builds on the paper Borri et al. (2018) and investigates the effect of different noise sources in a coarse-grained model of the interplay among growth rate, metabolism and resource allocation. Approximate moment computations and cross-correlation functions based on a Stochastic Hybrid System framework are validated via approximate stochastic simulations (τ-leaping and Euler-Maruyama), in order to evaluate how noise propagates in the metabolic pathway. The use of the model suggests new interpretations concerning how noise impacts from metabolism to cellular growth (or vice versa) and highlight how different noise sources could provide very different results in terms of noise propagation.

ACKNOWLEDGEMENTS

PP is supported by the SYSBIO.ISBE.IT within the Italian Roadmap for ESFRI Research Infrastructures. AS was supported by the National Science Foundation Grant ECCS 1711548.

REFERENCES

U. Alon (2019), "*An Introduction to Systems Biology: Design Principles of Biological Circuits*," Chapman and Hall/CRC, second edition

A. Borri, P. Palumbo, A. Singh (2016), "Impact of negative feedback in metabolic noise propagation," *IET Syst. Biol.*, 1-8.

A. Borri, P. Palumbo, A. Singh (2018), "Noise propagation in feedback coupling between cell growth and metabolic activity," *Proc. IEEE Conf. Decision & Control (CDC2018)*, Miami Beach, FL, USA, 2679–2684

D.T. Gillespie (1977), "Exact Stochastic Simulation of Coupled Chemical Reactions," *The Journal of Physical Chemistry*, 81(25), 2340-–2361

D.T. Gillespie (2001), "Approximate accelerated stochastic simulation of chemically reacting systems," *The Journal of Chemical Physics*, 115(4), 1716–1733

I. Golding, J. Paulsson, S. Zawilski, E. Cox (2005), "Real-time kinetics of gene activity in individual bacteria," *Cell* 123, 1025–1036

J.P. Hespanha, A. Singh (2005), "Stochastic models for chemically reacting systems using polynomial stochastic hybrid systems," *Int. J. of Robust and Nonlinear Control*, 15, 669–689

D.J. Higham (2001), "An algorithmic introduction to numerical simulation of stochastic differential equations," *SIAM Review*, 43, 525–546

D.J. Kiviet, P. Nghe, N. Walker, S. Boulineau, V. Sunderlikova, S.J. Tans (2014), "Stochasticity of metabolism and growth at the single-cell level," *Nature*, 514, 376–379.

I.T. Kleijn, L.H.J. Krah, R. Hermsen (2018), "Noise Propagation in an Integrated Model of Bacterial Gene Expression and Growth," *PLOS Computational Biology*, 14(10),): e1006386. https://doi.org/10.1371/journal.pcbi.1006386

S. Klumpp, Z. Zhang, T. Hwa (2009), "Growth Rate-Dependent Global Effects on Gene Expression in Bacteria," *Cell*, 139(7), 1366–1375

S. Modi, M. Soltani, A. Singh (2018), "Linear Noise Approximation for a Class of Piecewise Deterministic Markov Processes," *Proc Am Control Conf*, Milwaukee, US, 1993-–1998

N. Nordholt, J. van Heerden, R. Kort, F.J. Bruggeman, "Effects of growth rate and promoter activity on single-cell protein expression," *Scientific Reports*, 7:6299, DOI:10.1038/s41598-017-05871-3, 2018

A. Singh, P. Bokes (2012), "Consequences of mRNA Transport on Stochastic Variability in Protein Levels," *Biophysical J.*, 103, 1087-–1096

A. Singh, J.P. Hespanha (2011), "Approximate moment dynamics for chemically reacting systems," *IEEE Transactions on Automatic Control.* 56, 414–418

M. Soltani, T. Platini, A. Singh (2016), "Stochastic analysis of an incoherent feedforward genetic motif," *Proc Am Control Conf*, Boston, MA, USA, 406–411

M. Soltani, C. Vargas, A. Singh (2015), "Conditional moment closure schemes for studying stochastic dynamics of genetic circuits," *IEEE Transactions on Biomedical Circuits and Systems*, 9(4), 518–526

E. D. Sontag and A. Singh (2015), "Exact Moment Dynamics for Feedforward Nonlinear Chemical Reaction Networks," *IEEE Life Sciences Letters*, 1(2), 26–29

P. Thomas, G. Terradot, V. Danos, A.Y. Weiße (2018), "Sources, Propagation and Consequences of Stochasticity in Cellular Growth," *Nature Communications*, 9:4528. DOI: 10.1038/s41467-018-06912-9

M.K. Tonn, P. Thomas, M. Barahona, D.A. Oyarzun (2019), "Stochastic modelling reveals mechanisms of metabolic heterogeneity," *Communications Biology*, 2:108. https://doi.org/10.1038/s42003-019-0347-0

M. Wehrens, F. Buke, P. Nghe, S.J. Tans (2018), "Stochasticity in cellular metabolism and growth: Approaches and consequences," *Current Opinion in Systems Biology*, 8, 131-136

A.Y. Weiße, D.A. Oyarzun, V. Danos, P.S. Swain (2015), "Mechanistic links between cellular trade-offs, gene expression, and growth," *Proc Natl Acad Sci USA* 112(9), E1038–E1047